PERGAMON

Acta mater. 48 (2000) 1679–1689

Acta MATERIALIA

www.elsevier.com/locate/actamat

CRYSTALLOGRAPHY AND STRUCTURAL EVOLUTION DURING REVERSE TRANSFORMATION IN AN Fe–17Cr–0.5C TEMPERED MARTENSITE

D. V. SHTANSKY†‡, K. NAKAI and Y. OHMORI

Department of Materials Science and Engineering, Faculty of Engineering, Ehime University, 3 Bunkyo-cho, Matsuyama, 790-8577, Japan

(Received 8 October 1999; accepted 23 December 1999)

Abstract—The mechanism and the crystallography of austenite and δ-ferrite formation from tempered martensite at temperatures of 900–1200°C have been studied by means of transmission electron microscopy in an Fe–17Cr–0.55C alloy. It was found that austenite nucleates within ferrite at low angle, high angle and twin-related lath boundaries as well as at high angle equiaxed grain boundaries in contact with $M_{23}C_6$ grain/lath boundary carbides. The austenite grains are in a cube–cube relationship with the $M_{23}C_6$ carbide particles and bear the Kurdjumov–Sachs orientation relationship with at least one of the adjacent ferrite grains. They are often in the Kurdjumov–Sachs relationship with both ferrite laths separated by a high angle boundary as far as the laths had formed from the same austenite. The $\{111\}_A$ close packed plane of γ precipitate is parallel to the $\{110\}_F$ plane most parallel to the grain boundary. The close packed planes of some austenite grains nucleating at the high angle lath boundaries are parallel to the close packed planes of both ferrite laths. These crystallographic features often result in a single variant of austenite orientation at a grain boundary. After nucleation, the austenite grains grow by the migration of both semicoherent and incoherent interfaces. These results demonstrate that a specific orientation relationship is preferred for the austenite nucleation, but is not necessary for the subsequent growth. The kinetics of austenite growth are controlled by chromium diffusion. The δ-ferrite particles precipitate at high temperatures as a non-equilibrium phase. No rational orientation relationship between δ-ferrite and retained austenite was found. The experimental results are discussed qualitatively in terms of the thermodynamic predictions using the software ThermoCalc, assuming local equilibrium at the moving interfaces. © *2000 Acta Metallurgica Inc. Published by Elsevier Science Ltd. All rights reserved.*

Keywords: Phase transformations; Crystallography; Microstructure; Transmission electron microscopy (TEM); Phase diagrams

1. INTRODUCTION

This article is part of a systematic attempt to reveal the mechanism, the kinetics and the crystallography of reaustenitization processes in Fe–Cr–C alloys [1, 2]. The $\alpha \rightarrow \gamma$ transformation has been shown to be diffusion controlled, the kinetics of the reaction are very complex and the microstructural observations have been qualitatively interpreted assuming local equilibrium is maintained at the moving interfaces. The crystallography of the $\alpha \rightarrow \gamma$ transformation, however, has received less attention in comparison with that of the proeutectoid ferrite formation from austenite [3–7]. Law and Edmonds [8] reported that the austenite allotriomorphs nucleating on a ferrite grain boundary exhibited the Kurdjumov–Sachs orientation relationship with one of the ferrite grains, and grew into the adjacent grain by the migration of an incoherent interface. Shtansky *et al.* [2] showed that the austenite nucleating in contact with a pearlite did not have any reproducible orientation relationship with pearlitic ferrite, but both phases were occasionally related with the Kurdjumov–Sachs orientation relationship. It is thus questionable whether a rational orientation relationship is necessary between the austenite and ferrite grain in which it grows. The other point which has to be clarified is whether preferential austenite growth occurs into the incoherent ferrite grain. It should be noted that carbide particles situated on the grain boundaries provide the austenite nucleation sites and the growth of austenite is controlled by carbide dissolution. In such a case, the

† On leave from the I.P. Bardin Iron and Steel Industry Institute, 2nd Baumanskaya Street, 9/23, Moscow 107005, Russia, and now at the Department of Materials Science, Faculty of Engineering, University of Tokyo, 7-3-1 Hongo, Bunkyo-ku, Tokyo 113-8656, Japan.

‡ To whom all correspondence should be addressed.

PII: S1359-6454(00)00015-X

crystallography of grain boundary carbides may affect the austenite orientation since it can be related either to ferrite or carbide. In high Cr alloy, δ-ferrite is also allowed to form during austenitization. Despite this fact, little is known about the mechanism and the crystallography of δ-ferrite formation during heating compared with the ferrite precipitation during austenite decomposition.

The present study has been undertaken in order to reveal the crystallography and the structural evolution during heating in the tempered martensite of an Fe–17Cr–0.5C alloy by means of transmission electron microscopy. The mechanism and the kinetics of both austenite and δ-ferrite formation will be discussed assuming the reaction to be diffusion controlled and local equilibrium to be maintained at the moving interface.

2. EXPERIMENTAL PROCEDURE

The chemical composition of the alloy used in the present investigation is shown in Table 1. Specimens of 20 mm in diameter and 10 mm long were austenitized at 1250°C for 15 min in a dynamic argon atmosphere and quenched into iced brine to produce martensite. Then these specimens were encapsulated in evacuated quartz tubes and tempered at 735°C for 240 h. This heat treatment resulted in the initial microstructure consisting of spherical or globular $M_{23}C_6$ carbide particles and fully tempered ferrite matrix. Two ferrite grain morphologies were observed: the lath morphology with its parallel sub-units and the equiaxed ferrite grains [2]. Sheets $10 \times 10 \times 0.3$ mm^3 in size were sliced from the center of the heat-treated specimens, austenitized at various temperatures in the range of 900–1200°C for 1–100 s, and then quenched into iced brine. Thin foils for TEM studies were prepared using a standard technique involving mechanical grinding to a thickness of 0.08 mm on both surfaces to remove outer oxidized layers and electropolishing by a conventional twin-jet polishing method using an electrolyte containing 10% perchloric acid, 20% glycerol and 70% ethanol. Thin films were examined in a JEM-3010 transmission electron microscope operating at 300 kV.

3. EXPERIMENTAL RESULTS

3.1. Austenite/carbide orientation relation

The austenite formed at 900°C was found to transform completely into martensite during quenching, but it was retained after short austenitizing times at higher temperatures. Figure 1 shows the retained austenite region which formed when austenitized at 1200°C for 10 s in contact with an undissolved $M_{23}C_6$ carbide particle. This austenite was probably of high carbon and chromium content, as reported previously [1, 9]. Both phases obey a cube–cube orientation relationship (OR), as in many other results [10–12]. Since the OR between austenite and martensite can be expressed by either the Kurdjumov–Sachs [13] or the Nishiyama–Wasserman [14, 15] relationship, the Kurdjumov–Sachs OR between austenite and martensite and a cube–cube OR between austenite and $M_{23}C_6$ carbide will be employed in the present study in order to evaluate the crystallography of austenite.

Table 1. Chemical composition of the alloy (mass%)

C	Si	Mn	P	S	Cr	N	O	Al
0.54	0.02	0.02	0.001	0.001	17.09	0.0036	0.002	0.001

3.2. Crystallography of austenite formation

3.2.1. Low angle lath boundary. Figure 2(a) shows the nucleation of austenite at a low angle lath boundary in the specimen heat treated at 900°C for 10 s. The selected area electron diffraction (SAED) patterns taken from the ferrite/carbide and martensite/carbide areas allow the crystallography of coexisted phases to be determined. The stereographic analysis for these diffraction patterns is shown in Fig. 2(b). The incident beam direction is $[115]_{F1,\ F2,\ M2}//[\bar{3}2\bar{1}]_C//[112]_{M1}//[113]_{M3}$ (hereafter, the subscripts F, M, A and C denote ferrite, martensite, austenite and $M_{23}C_6$ carbide, respectively). Since the ferrite laths were found to be of almost the same orientation, this type of boundary can be simply considered as an array of dislocations. The stereographic analysis shows that the $M_{23}C_6$ carbide particles were related to the ferritic matrix by the Kurdjumov–Sachs OR. Since the austenite forming at 900°C transformed into martensite completely during quenching, three different martensite orientation variants were recognized. All of them exhibited the Kurdjumov–Sachs OR with the $M_{23}C_6$ carbides, and one of the martensite crystals was in the same orientation with the initial ferrite.

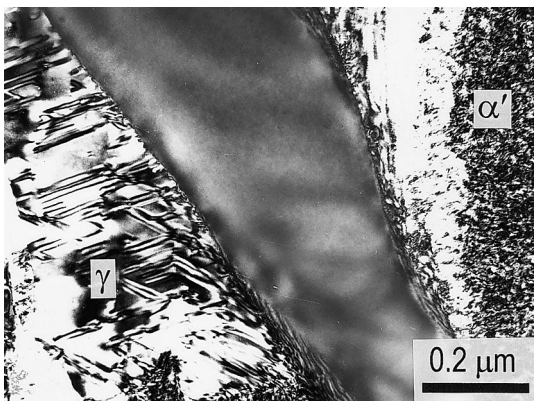

Fig. 1. Bright field TEM micrograph showing the retained austenite after heat treatment at 1200°C for 10 s.

If the orientation of austenite is deduced by assuming the austenite/martensite and austenite/carbide ORs, the austenite will unambiguously be related to the ferrite and the $M_{23}C_6$ carbides with the Kurdjumov–Sachs OR and a cube–cube OR, respectively. This implies that the austenite/ferrite interface was semicoherent on both sides of the low angle lath boundary. The austenite grew predominantly along the sub-boundary into both ferrite laths. It is interesting to note that the low angle grain boundary plane was close to the close packed $\{111\}_{A,\,C}//\{110\}_{F,\,M}$ plane, in keeping with the suggestion by Lee and Aaronson [16, 17].

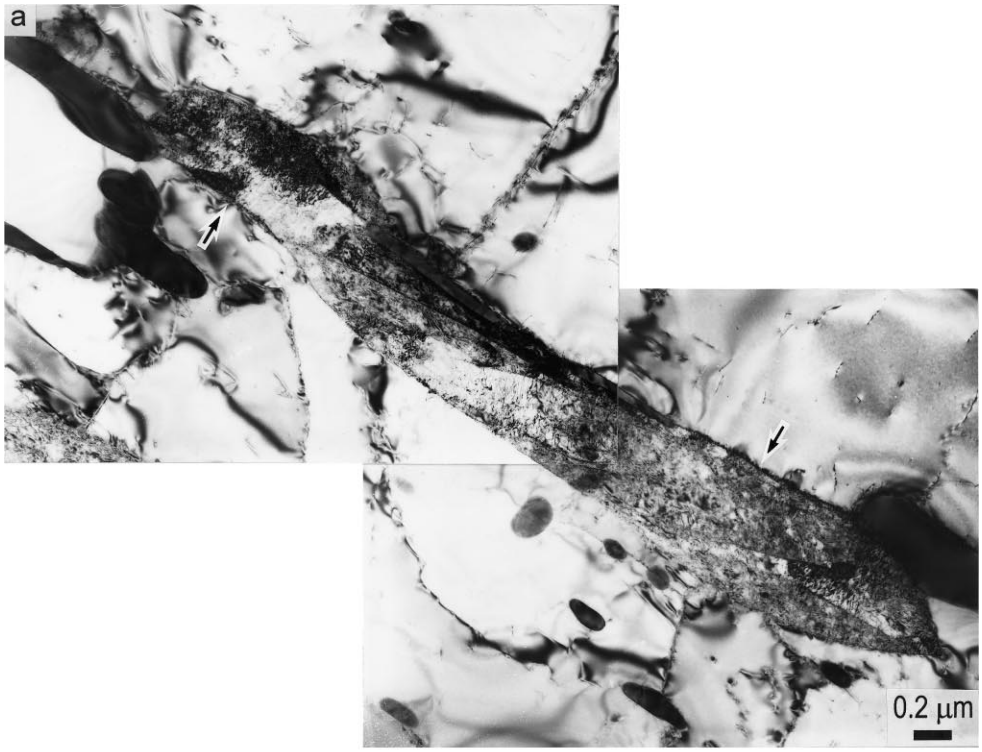

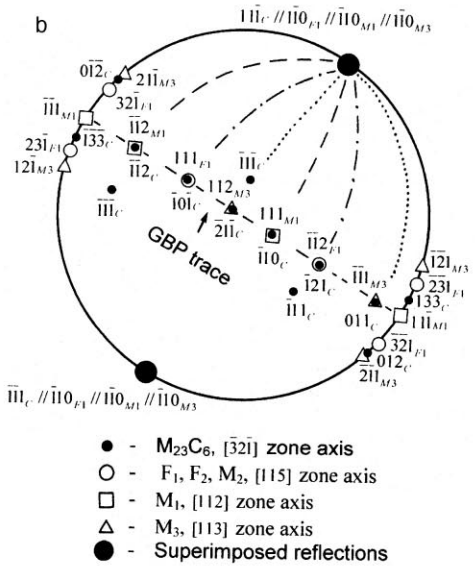

Fig. 2. (a) Bright field TEM micrograph showing the nucleation of austenite at the low angle lath boundary after heating at 900°C for 10 s. (b) The $[115]_{F1,\,F2,\,M2}//[\bar{3}2\bar{1}]_{M23C6}//[112]_{M1}//[113]_{M3}$ stereographic projection showing the ORs between ferrite, martensite and $M_{23}C_6$ carbide. Arrows indicate (a) the prior low angle boundary position and (b) the trace of the grain boundary plane (GBP).

3.2.2. Twin-related lath boundary. Figure 3(a) shows the austenite grain (austenite transformed into martensite completely during subsequent quenching) which nucleated in contact with the $M_{23}C_6$ carbide located on a twin-related lath boundary and grew into one of the ferrite laths. The $[9\bar{3}2]_C//[\bar{1}\bar{3}\bar{5}]_{F1}//[135]_{F2}//[320]_M$ stereographic projection is shown in Fig. 3(b). The $M_{23}C_6$ carbide particle related to both the ferrite laths and the martensite by the Kurdjumov–Sachs OR. Thus the orientation of the parent austenite was deduced to be in the Kurdjumov–Sachs relationship with all the b.c.c. crystals observed and in a cube–cube relationship with the $M_{23}C_6$ carbide. Although in this particular case the lath boundary was slightly curved, the boundary plane was close to $\{111\}_{A,\,C}//\{110\}_{F1,\,F2,\,M}$, within 10°. Despite the fact that the ferrite/austenite interface was semicoherent on both sides of the lath boundary, the austenite precipitate only grew into one of the ferrite laths.

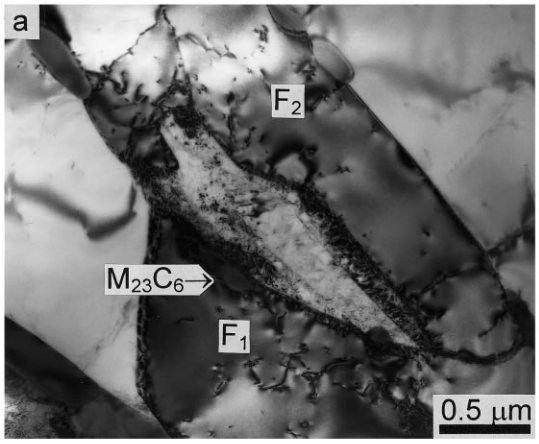

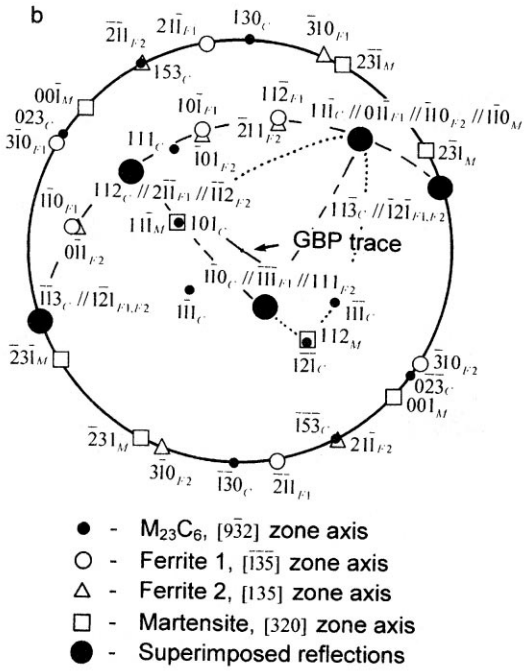

Fig. 3. (a) Bright field TEM micrograph showing an austenite nucleation at a twin lath boundary after heating at 900°C for 15 s. (b) The $[9\bar{3}2]_{M23C6}//[\bar{1}\bar{3}\bar{5}]_{F1}//[135]_{F2}//[320]_M$ stereographic projection showing the ORs between ferrites, martensite and $M_{23}C_6$ carbide. The arrow indicates the trace of the GBP.

3.2.3. High angle lath boundary formed from an austenite grain. Figure 4(a) shows the austenite grain that spread along a high angle lath boundary. Two ferrite laths were tilted about the common $[\bar{1}10]$ axis with an angle of 19.5°. By examining the corresponding SAED patterns, the $M_{23}C_6$ carbide particles located on the lath boundary were related to both the ferrite grains by different variants of the Kurdjumov–Sachs OR, showing that both the laths were formed from the same austenite grain. Within the transformed region three martensite orientations were recognized. Figure 4(b) represents the $[\bar{3}2\bar{1}]_C//[112]_{F1}//[115]_{F2,\,M3}//[33\bar{5}]_{M1}//[110]_{M2}$ stereographic projection. The martensite orientation 3 was similar to that of the ferrite grain 1 and the martensite orientation 1 was close to that of the ferrite grain 2. All the martensite crystals obeyed the Kurdjumov–Sachs OR with respect to the $M_{23}C_6$ carbide. Again the crystallography between ferrite, martensite and carbide allows the orientation of austenite to be determined. The stereographic projection shows that the two specific ORs reported above are fulfilled between the austenite and initial phases. Hence, as in the previous cases, the austenite nucleated at a high angle lath boundary in contact with the $M_{23}C_6$ carbide particle and bore the Kurdjumov–Sachs OR with both ferrite laths, the austenite being related to the $M_{23}C_6$ carbide by a cube–cube OR. The high angle lath boundary plane was parallel to $\{111\}_{A,\,C}//\{110\}_{F1,\,F2,\,M1-3}$. The austenite grew preferentially into one of the ferrite laths by the migration of a semicoherent interface, keeping a good coherency with the opposite ferrite lath as well. The ferrite/austenite interface was curved on both sides of the lath boundary in keeping with previous results [1, 2], but the present result appears different from that of Ryder and Pitsch [3]. They observed that the ferrite particles with straight interfaces always exhibited a specific OR with the austenite grain into which they were growing, while the particles with curved interfaces did not exhibit any OR with the austenite grain into which they were growing.

Figure 5 is also the case where the austenite nucleated at a high angle ferrite lath boundary and grew into both the ferrite laths by the migration of semicoherent interfaces. Both the ferrite laths were related to the $M_{23}C_6$ carbides located on the lath boundary by different variants of the Kurdjumov–Sachs OR. The martensite orientations 1 and 2

were similar to those of the ferrite laths 1 and 2, respectively. Hence, the austenite grain nucleated at the high angle lath boundary was Kurdjumov–Sachs related to both ferrite laths and bore a cube–cube OR with respect to the $M_{23}C_6$ carbides, indicating that both ferrite laths nucleated within an austenite grain. The stereographic analysis shows that the lath boundary plane was close to $(\bar{1}1\bar{1})_{A,\,C}//(01\bar{1})_{F1}$, in keeping with the results of Ameyama *et al*. [18].

3.2.4. High angle equiaxed grain boundary. In the examples considered above, an austenite nucleating at a lath boundary held a specific orientation relationship with respect to both ferrite laths, as far as the laths had formed from the same austenite.

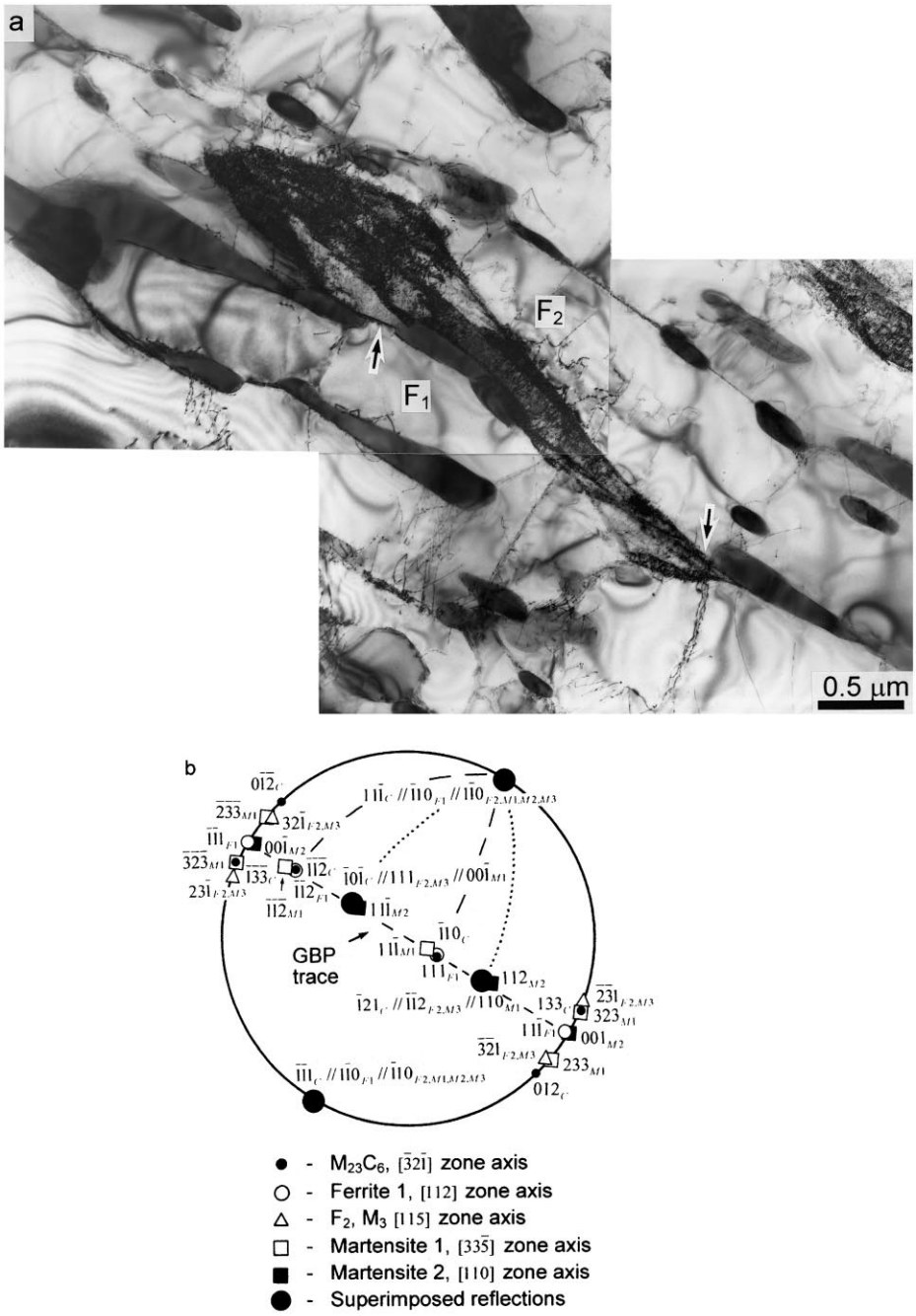

Fig. 4. (a) Bright field TEM micrograph showing the nucleation of austenite at a high angle lath boundary after heating at 900°C for 10 s. (b) The $[\bar{3}2\bar{1}]_{M23C6}//[112]_{F1}//[115]_{F2,\,M3}//[33\bar{5}]_{M1}//[110]_{M2}$ stereographic projection showing the ORs between ferrites, martensite and $M_{23}C_6$ carbide. Arrows indicate (a) the prior high angle boundary position and (b) the trace of the GBP.

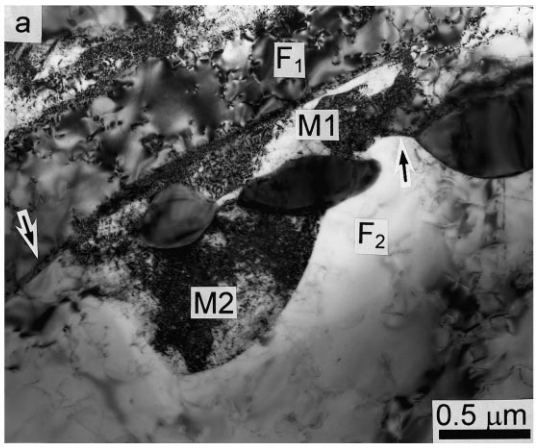

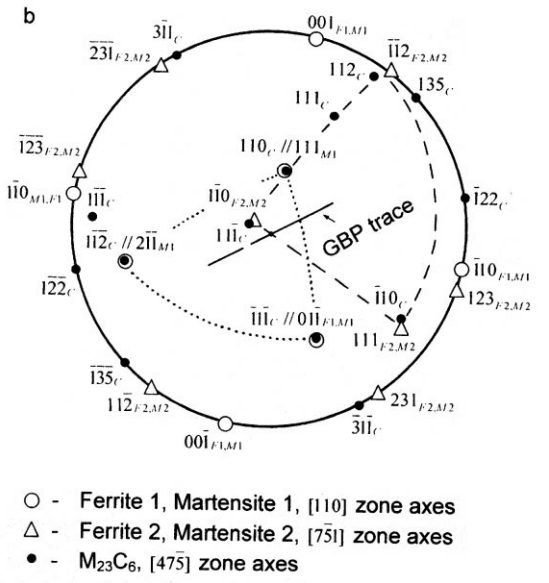

Fig. 5. (a) Bright field TEM micrograph showing the nucleation of austenite at a high angle lath boundary after heating at 900°C for 25 s. (b) The $[47\bar{5}]_{M23C6}//[110]_{F1,\,M1}//[7\bar{5}1]_{F2,\,M2}$ stereographic projection showing the ORs between ferrites, martensite and $M_{23}C_6$ carbide. Arrows indicate (a) the prior high angle boundary position and (b) the trace of the GBP.

Figure 6 is an example of when the austenite precipitate grew into one ferrite grain with an incoherent interface, although an orientation relationship existed with the adjacent grain. The austenite particle nucleating in the vicinity of both the $M_{23}C_6$ carbide and a grain boundary triple point appears to be unconnected with them, although this observation could be an artifact of sectioning. The $M_{23}C_6$ carbide was in the Kurdjumov–Sachs relation with the ferrite grain 2, although it did not exhibit any rational OR with respect to the opposite grain 1. The orientation of the martensite crystal was similar to that of the ferrite grain 2, in which the austenite did not grow. Since an austenite transforms into martensite via either the Kurdjumov–Sachs or the Nishiyama–Wasserman OR, the orientation of the present austenite with respect to the ferrite grain 2 was probably the same. No rational OR was found between the austenite and ferrite grain into which the austenite grew. Thus, an austenite grain precipitating at a high angle grain boundary grew into ferrite by the migration of an incoherent interface at least at 950°C. This particular observation supports the hypothesis originally proposed by Smith [19] and confirmed by other works [7, 8], that a grain boundary precipitate should grow preferentially into the grain with which no coherent interface is formed. Note that the grain boundary plane was parallel to $(111)_{A,\,C}//(\bar{1}01)_{F2,\,M}$.

Figure 7(a) shows the austenite grain (austenite

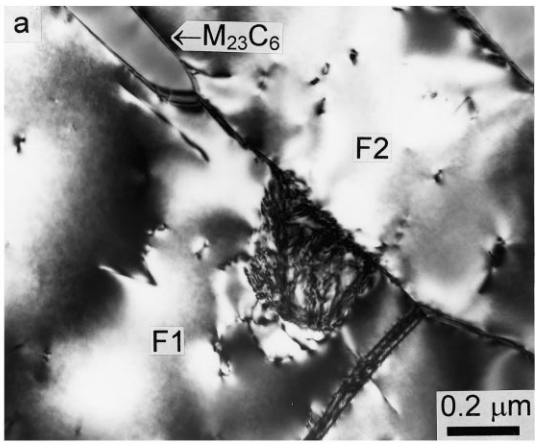

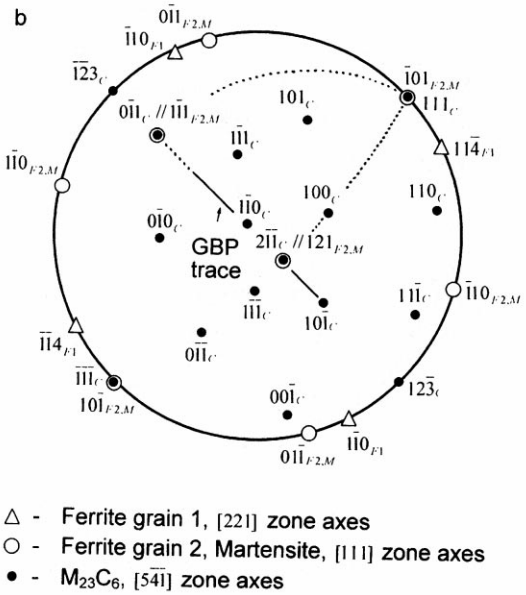

Fig. 6. (a) Bright field TEM micrograph showing the nucleation of austenite at a high angle grain boundary after heating at 900°C for 15 s. (b) The $[5\bar{4}\bar{1}]_{M23C6}//[221]_{F1}//[111]_{F2,\,M}$ stereographic projection showing the ORs between the ferrite, martensite and $M_{23}C_6$ carbide. The arrow indicates the trace of the GBP.

completely transformed into martensite during subsequent quenching), which spread from a high angle grain boundary into both the ferrite grains. Analysis of the SAED patterns revealed that the $M_{23}C_6$ carbide particle located on the grain boundary was not related to either ferrite grain by a specific OR. A twin relation can be recognized between two martensite crystals within the transformed austenite region. If the twin-related martensite crystals are assumed to arise from a single austenite with the Kurdjumov–Sachs OR, the variant of the Kurdjumov–Sachs OR between the austenite and ferrite grain 1 could be expected within a few degrees. The variant selection resulting in the smallest misorientation between the $(1\bar{1}\bar{1})_A$ close packed plane of the grain boundary austenite and the $(1\bar{1}0)_{F2}$ plane of the ferrite grain 2 is shown in the stereographic projection [Fig. 7(b)]. No rational OR between the austenite and either the ferrite grain 2 or the $M_{23}C_6$ carbide particle was found. It can be seen that the austenite grew into both the ferrite grains by the migration of semicoherent (fer-

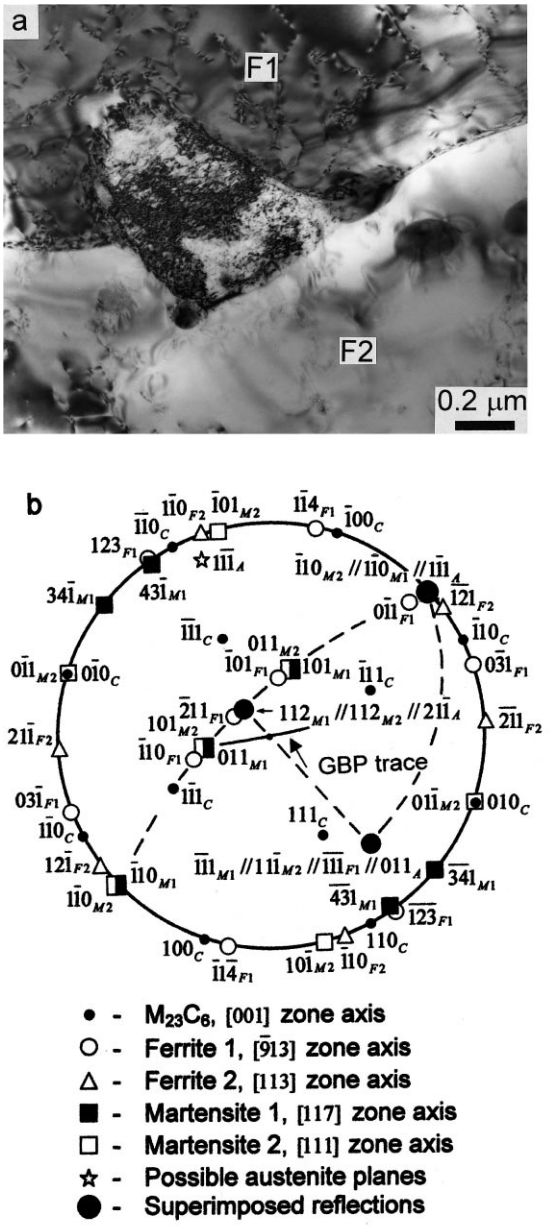

Fig. 7. (a) Bright field TEM micrograph showing the nucleation of austenite at a high angle grain boundary after heating at 900°C for 60 s. (b) The $[001]_{M23C6}//[\bar{9}13]_{F1}//[113]_{F2}//[117]_{M1}//[111]_{M2}$ stereographic projection showing the ORs between ferrites, austenite, martensite and $M_{23}C_6$ carbide. The arrow indicates the trace of the GBP.

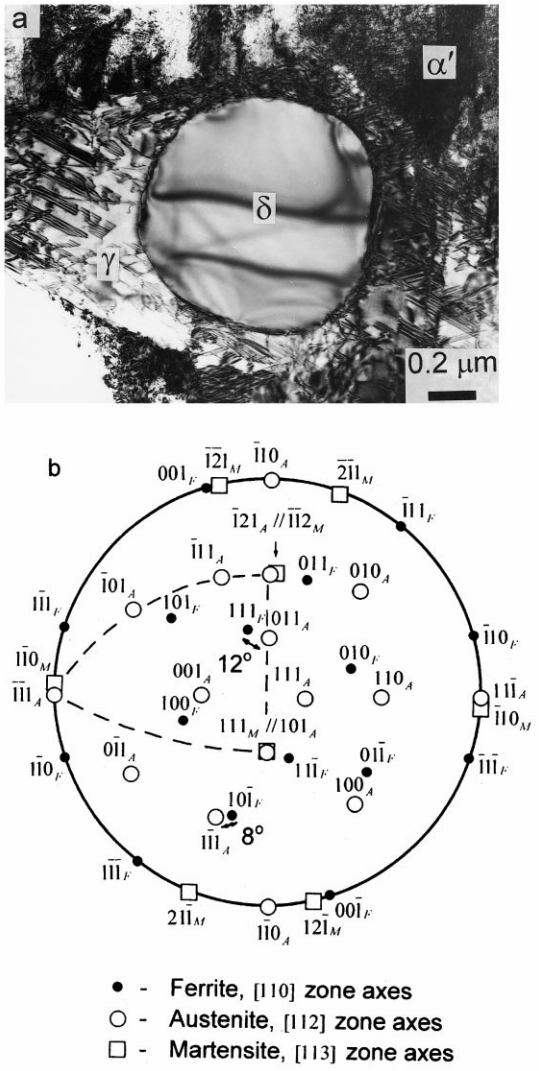

Fig. 8. (a) TEM micrograph showing the δ-ferrite precipitate within the retained austenite after heat treatment at 1200°C for 10 s. (b) The $[110]_F//[112]_A//[113]_M$ stereographic projection showing the Kurdjumov–Sachs OR between the austenite and martensite. Low index axes of the austenite and δ-ferrite are plotted. Note that the δ-ferrite orientation largely deviates from the Kurdjumov–Sachs OR with respect to the austenite.

rite grain 1) and incoherent (ferrite grain 2) interfaces.

3.3. δ-Ferrite precipitation

The δ-ferrite is precipitated by austenitization at higher temperatures. Thermodynamic calculations using Thermo-Calc software [20] shows that the composition of the alloy falls into a γ single-phase field at 1200°C. Moreover, structural examination after the austenitization at 1200°C for 15 min showed that the δ-ferrite particles were completely dissolved in the austenite. Thus, δ-ferrite is not an equilibrium phase at this temperature. Figure 8(a) shows the δ-ferrite precipitate within the austenite after heating at 1200°C for 10 s. The shape of the δ-ferrite is spherical with a particle size of about 1 μm. Since the δ-ferrite was dislocation free, it is likely that the ferrite formed at a high temperature. This specific feature distinguishes it from the untransformed ferrite that was observed after a short austenitizing time (Fig. 9).

It is well established that a precipitate usually has a specific orientation relationship with the matrix. It is, however, surprising that no rational OR between δ-ferrite and the surrounding austenite was found. Figure 8(b) is the $[110]_F//[112]_A//[113]_M$ stereographic projection, where the planes of low indexes in ferrite and austenite are plotted. The retained austenite as was expected to be Kurdjumov–Sachs related with the martensite crystal. The OR between the δ-ferrite and the surrounding austenite is irrational, with a scatter larger than 15° from the Kurdjumov–Sachs relationship. In total, four cases were analyzed and at least three of them are different from the Kurdjumov–Sachs OR. Thus, in this case, the f.c.c. and b.c.c. crystals were in a random orientation. Since the interfacial energy should be high, the equilibrium shape of the precipitate will be roughly spherical [21], in keeping with the present results.

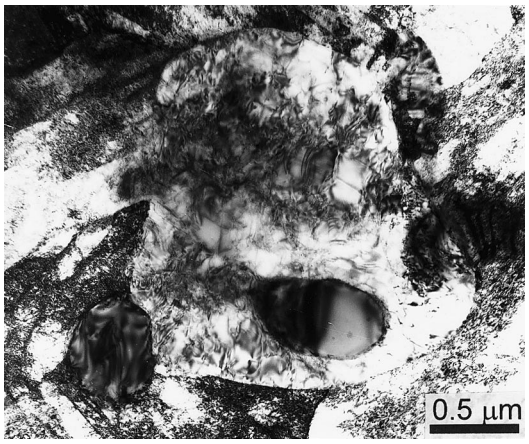

Fig. 9. TEM micrograph showing the untransformed ferrite region after heat treatment at 1200°C for 6 s.

4. DISCUSSION

4.1. Crystallography

In the present study, a grain boundary austenite precipitate had the Kurdjumov–Sachs OR with at least one of the ferrite matrix grains. This result agrees well with the studies on grain boundary precipitates in a number of systems, for instance in a low carbon steel [7], Co–Fe alloy [22], duplex stainless steel [18], titanium alloy [23] and Ni–Cr alloy [24]. Since an austenite almost always nucleates in contact with lath or grain boundary $M_{23}C_6$ carbides, it selects a cube–cube OR with these carbides. It was frequently observed that an austenite was in the Kurdjumov–Sachs OR with both ferrite laths which had formed from a single austenite as in previous results [7, 22, 23]. Such a variant selection occurs to minimize the interface energy between all phases having a common interface.

Ameyama *et al.* [18] reported that the $\{111\}_A$ plane of grain boundary γ in α/γ duplex stainless steels was parallel to the $\{110\}_F$ close-packed α planes most parallel to the grain boundary. Lee and Aaronson [16, 17] also suggested that a low energy interface should be parallel to the grain boundary as much as possible, whereas King and Bell [7] concluded that the orientation of the boundary plane does not directly influence the OR. Furuhara *et al.* [23] reported a rule of variant selection in a β titanium alloy resulting in the smallest misorientation angle between the parallel close packed directions and the grain boundary plane. The crystallographic feature of austenite formation in the present study can be summarized as follows.

1. The austenite nucleated at a low angle or twin-related ferrite lath boundary holds the Kurdjumov–Sachs and cube–cube ORs with respect to the ferrite and $M_{23}C_6$ carbide particle locating on this lath boundary, respectively. The $\{111\}_{A,C}//\{110\}_F$ close packed plane was almost parallel to the lath boundary (Figs 2 and 3).
2. The austenite nucleated at a high angle lath boundary was related by the Kurdjumov–Sachs OR to both ferrite laths and by a cube–cube OR to the $M_{23}C_6$ lath boundary carbide. The $\{111\}_A$ plane of γ precipitate was parallel to the $\{110\}_F$ plane of either one or both ferrite laths, also being parallel to the lath boundary (Figs 4 and 5).
3. The austenite nucleating at a high angle equiaxed grain boundary holds the Kurdjumov–Sachs OR with one of the ferrite grains and can occasionally be related by a cube–cube OR to the $M_{23}C_6$ grain boundary carbide. The $\{111\}_A$ close packed plane of the γ precipitate, which was related to one of the ferrite grains by the Kurdjumov–Sachs OR, was found to be parallel to the grain boundary (Figs 6 and 7).

From the results obtained, it can be concluded that

neither a specific OR resulting in a low energy semi-coherent interface nor an incoherency is necessary for the subsequent austenite growth. It has been reported that the preferential growth of precipitate takes place into the grain with which it did not have any orientation relationship [7, 8]. The present study is in contradiction with this deduction. It is likely that an austenite can start to grow initially into the grain with which it is not related (Fig. 6), but it can also continue to grow into the opposite grain (the related one) (Fig. 7). The grain boundary austenite often grew only into one of the ferrite grains, even when it was related to both grains. Thus in the case under consideration, an austenite grain nucleates within a ferrite grain on a boundary and preferentially grows into this grain. The present results support the conclusion by King and Bell [7] that a specific OR is preferred for the nucleation of precipitate, but is not necessary for the subsequent growth. It was frequently observed that the martensite, which is the decomposition product of austenite growing into the ferrite grain, possessed the same orientation with this ferrite. Hence, in this case, the martensite obeyed the same variant of the Kurdjumov–Sachs OR with the austenite as between the ferrite and the austenite.

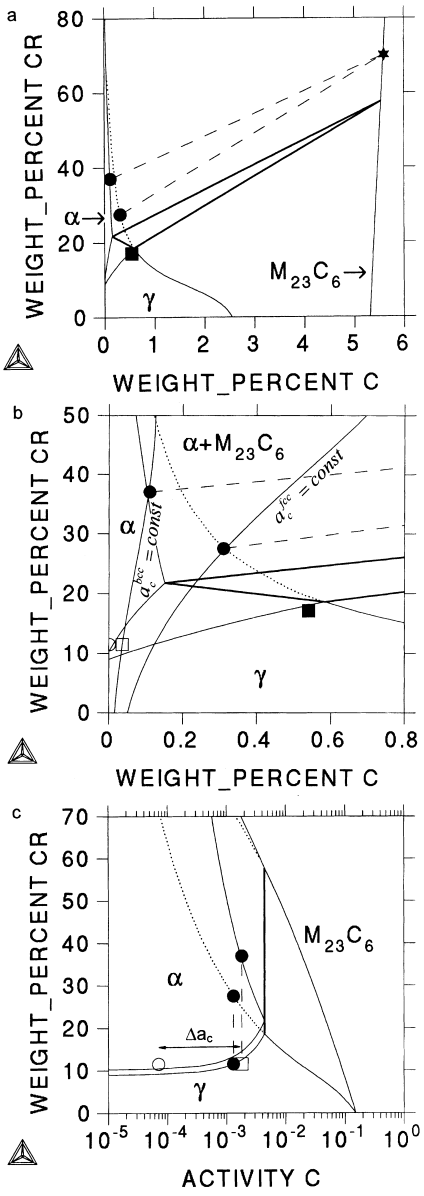

Fig. 10. Calculated isothermal section of the Fe–Cr–C phase diagram at 1200°C representing the metastable three-phase equilibrium between α, γ and $M_{23}C_6$ carbide with wt% carbon (a), (b), and carbon activity (c) as horizontal axes. The dotted line shows the calculated metastable extension of the $\gamma + M_{23}C_6$ two-phase equilibrium. The two broken lines represent the tie-lines of the $\alpha + M_{23}C_6$ and $\gamma + M_{23}C_6$ equilibria. The composition of the alloy is marked by a filled square (■). All the other lines and symbols are explained in Section 4.2.

It has been shown that both sides of the grain boundary precipitate contained ledges and misfit compensation defects, resulting in a partially coherent interface, even when it was irrationally related [24, 25]. In the present study, the subsequent martensite transformation destroyed the shape of the α/γ interface and it is thus difficult to see whether the interface was smooth or faceted.

4.2. *Thermodynamical consideration*

The austenite in an Fe–17Cr–0.5C alloy was found to nucleate after some incubation time, as in previous results [1, 2, 26]. Two specific features of the microstructural evolution should also be mentioned. Some parts of the ferritic matrix were observed to remain untransformed, even after rather long austenitization times, 100 s at 900°C or 15 s at 1200°C. Another interesting observation is that δ-ferrite precipitates within an austenitic matrix as a non-equilibrium phase. In order to understand these phenomena qualitatively, it is useful to examine the corresponding phase diagram assuming that local equilibrium is maintained at the moving interfaces [1, 2].

Figure 10 shows the calculated isothermal section of the Fe–Cr–C phase diagram at 1200°C, representing the metastable $\alpha + \gamma + M_{23}C_6$ three-phase equilibrium with different axes. The dotted line represents the calculated metastable extension of the $\gamma + M_{23}C_6$ two-phase equilibrium. The initial compositions of ferrite and $M_{23}C_6$ carbide after tempering at 735°C for 240 h are shown by an open circle (○) in Fig. 10(b) and a star (✱) in Fig. 10(a), respectively. The two broken tie-lines starting from the star define the equilibria at 1200°C between the $M_{23}C_6$ carbide and ferrite, and between the $M_{23}C_6$ carbide and austenite, marked by filled circles (●). The filled square (■) denotes the composition of the alloy investigated.

Figure 10(b) shows that the composition of the

initial ferrite falls inside the α single-phase field at 1200°C, indicating that ferrite is stable at this temperature. However, the composition of the initial ferrite close to the grain boundary, which is the preferential nucleation site for austenite, may fall well above the α/γ boundary because of the chromium adsorption in the grain boundary. The $\alpha \rightarrow \gamma$ transformation will only occur if the composition of ferrite shifts into the $\alpha+\gamma$ two-phase region. Figure 10(c) shows that the carbon activity difference Δa_c between the $\alpha/M_{23}C_6$ interface and the bulk α results in carbon diffusion. During this stage, the carbon activity of the matrix approaches the activity level at the $\alpha/M_{23}C_6$ interface to meet the thermodynamic requirement for the austenite nucleation. In view of the very high mobility of carbon at 1200°C, it is expected that the first stage will be complete almost instantaneously.

The driving force sufficient for chromium diffusion will be given at the beginning of the reaction. Thus, the ferritic matrix in the vicinity of the $M_{23}C_6$ carbide will be enriched in chromium as long as the matrix remains ferrite. The composition of ferrite varies along the isoactivity line $a_c^{b.c.c.} =$ const [see Fig. 10(b)]. An approximation of chromium diffusion distance obtained by the Einstein formula $x = 2\sqrt{Dt}$ is 1.7 μm for 1 s at 1200°C. Since the ferrite composition falls close to the α single-phase boundary it seems reasonable to assume that some parts of the ferritic matrix in the vicinity of the carbides will be enriched in chromium during the incubation time for austenite nucleation. Hence, these ferrite areas will not transform into austenite; this assumption agrees well with experimental observations.

Figure 10(c) shows the carbon activities at the $\alpha/M_{23}C_6$ and $\gamma/M_{23}C_6$ interfaces (●) as well as in the bulk ferrite (□) after austenite nucleation. It can be seen that the carbon activity at the $\gamma/M_{23}C_6$ interface is lower than that in the matrix, thus the $\alpha \rightarrow \gamma$ transformation will be controlled by chromium diffusion. Figure 10(c) also shows that the chromium composition in austenite at the $\gamma/M_{23}C_6$ interface falls inside the α single-phase field at 1200°C. Hence, ferrite is allowed to form within the high chromium austenite region during the reverse transformation. The crystalline orientation of δ-ferrite precipitated at 1200°C was not related to austenite. At such a high temperature diffusion occurs rapidly and the interface mobility is very high. If the driving force is high enough to permit nucleation and growth of the incoherent interface, the $\gamma \rightarrow \delta$ transformation can only proceed by diffusion transformation.

5. SUMMARY

The mechanism and the crystallography of austenite formation from the tempered martensite in an Fe–17Cr–0.5C alloy were investigated by means of TEM. The following results were obtained.

1. Austenite nucleated after the incubation time, 10–60 s at 900°C, at low angle, high angle and twin-related lath boundaries, and high angle equiaxed grain boundaries in contact with $M_{23}C_6$ grain/lath boundary carbides. The ferritic matrix in the vicinity of the $M_{23}C_6$ carbide particles was being enriched in chromium during the incubation time, and the $\alpha \rightarrow \gamma$ transformation in these regions was much retarded.
2. The austenite precipitates possessed the Kurdjumov–Sachs OR with respect to at least one ferrite grain and a cube–cube OR with a $M_{23}C_6$ grain boundary carbide. The γ particles nucleated at a high angle lath boundary frequently had the Kurdjumov–Sachs OR with both matrix laths.
3. The $\{111\}_{A,C}//\{110\}_F$ close packed plane of austenite precipitate, $M_{23}C_6$ grain boundary carbide and at least one ferrite grain were almost parallel to the grain boundary. The close packed plane of γ precipitate formed at several of the high angle lath boundaries was parallel to both the grain boundary plane and the close packed planes of the adjacent matrix laths, as far as the laths had formed from a single austenite. These crystallographic features restricted the variant selection of γ grain boundary precipitate orientation.
4. The growth of austenite particles occurred into both matrix grains by the migration of semicoherent and incoherent interfaces. This result implies that a specific orientation relationship is not necessary for the subsequent austenite growth. The kinetics of austenite growth are controlled by chromium diffusion.
5. The δ-ferrite particles precipitated within austenite during austenitization at 1200°C. They were spherical in shape and dislocation free. No rational OR between austenite and δ-ferrite was found.
6. The mechanism and the kinetics of the structural evolution can be qualitatively understood by driving force determination using the calculated phase diagram. The local equilibrium hypothesis was assumed.

Acknowledgements—D.S. acknowledges the support of the Japan Society for the Promotion of Science during this work. This research was supported by a Grant-in-Aid from the Ministry of Education, Science, Culture and Sports. Thanks are also due to Sumitomo Metal Industries for supplying the materials used in the present study.

REFERENCES

1. Shtansky, D. V., Nakai, K. and Ohmori, Y., *Z. Metallkd.*, 1999, **90**, 25.

2. Shtansky, D. V., Nakai, K. and Ohmori, Y., *Acta mater*., 1999, **47**, 2619.
3. Ryder, P. L. and Pitsch, W., *Acta metall*., 1966, **14**, 1437.
4. Aaronson, H. I., in *AIME Symposium, Decomposition of Austenite by Diffusional Processes*, ed. V. F. Zackay and H. I. Aaronson. Interscience Publishers, 1962, p. 387.
5. Hillert, M., in *AIME Symposium, Decomposition of Austenite by Diffusional Processes*, ed. V. F. Zackay and H. I. Aaronson. Interscience Publishers, 1962, p. 197.
6. Smith, C. S., in *AIME Symposium, Decomposition of Austenite by Diffusional Processes*, ed. V. F. Zackay and H. I. Aaronson. Interscience Publishers, 1962, p. 237 (discussion of Hillert [5]).
7. King, A. D. and Bell, T., *Metall. Trans*., 1974, **6A**, 1419.
8. Law, N. C. and Edmonds, D. V., *Metall. Trans*., 1980, **11A**, 33.
9. Howell, P. R., Bee, J. V. and Honeycombe, R. W. K., *Metall. Trans*., 1979, **10A**, 1213.
10. Pumphrey, P. H. and Edington, J. W., *Acta metall*., 1994, **22**, 89.
11. Leitnaker, J. M. and Bentley, B., *Metall. Trans*., 1977, **8A**, 1605.
12. Southwick, P. D. and Honeycombe, R. W. K., *Metal. Sci*., 1982, **16**, 475.
13. Kurdjumov, G. V. and Sachs, G., *Z. Phys*., 1930, **64**, 325.
14. Nishiyama, Z., *Sci. Rep. Tohoku Univ*., 1934, **23**, 637.
15. Wasserman, G., *Arch. EisenhuttWes*., 1933, **16**, 647.
16. Lee, J. K. and Aaronson, H. I., *Acta metall*., 1975, **23**, 799.
17. Lee, J. K. and Aaronson, H. I., *Acta metall*., 1975, **23**, 809.
18. Ameyama, K., Maki, T. and Tamura, I., *J. Jpn. Inst. Met*., 1986, **50**, 602.
19. Smith, C. S., *Trans. Am. Soc. Met*., 1953, **45**, 533.
20. Hillert, M., in *Proc. Int. Conf. on Solid–Solid Phase Transf*. TMS-AIME,Warrendale, PA, 1981, p. 789.
21. Porter, D. A. and Easterling, K. E., in *Phase Transformation in Metals and Alloys*. Chapman & Hall, London, 1992, p. 152.
22. Ryder, P. L., Pitsch, W. and Mehl, R. F., *Acta metal*., 1967, **15**, 1431.
23. Furuhara, T., Takagi, S., Watanabe, H. and Maki, T., *Metall. Mat. Trans*., 1996, **27A**, 1635.
24. Furuhara, T. and Maki, T., *Mater. Trans., JIM*, 1992, **33**, 734.
25. Furuhara, T. and Aaronson, H. I., *Acta metal. mater*., 1991, **39**, 2887.
26. Shtansky, D. V. and Inden, G., *Acta mater*., 1997, **45**, 2879.